UDK 544.228
Original scientific article/Izvirni znanstveni članek

ISSN 1580-2949
MTAEC9, 57(1)3(2023)

POTENTIAL BARRIER ESTIMATION WITH A GRAPHICAL METHOD

GRAFIČNA OCENA POTENCIALA PREGRADE NA MEJAH KRISTALNIH ZRN

Souad Merabet[1,*], Bilal Djellil[2]

[1]University of Jijel, Department of Electronics, Laboratory of Renewable Energy, Jijel, Algeria
[2]University of Jijel, Department of Electronics, Laboratory of the Materials Studies, Jijel, Algeria

Prejem rokopisa – received: 2022-09-23; sprejem za objavo – accepted for publication: 2022-11-17

doi:10.17222/mit.2022.628

In this work, a representative graphical method was used to estimate the potential barrier at grain boundaries in polycrystalline materials. The used equation for the determination of trapping density states is closely related to the doping concentration in the layer. The obtained results showed that this density is a crucial parameter for estimating the maximum barrier value. This parameter strongly depends on the grain size and, consequently, on the grain boundary width. The conduction (or transport) properties represented by the thermionic current and the effective mobility also prove this dependence. Also, the obtained results are in good agreement with the experientially measured values from previous works.

Keywords: traps, charge carrier, dopant concentration, grain size

V članku je predstavljena izbrana grafična metoda za oceno potenciala pregrade na mejah kristalnih zrn v polikristalnih materialih. Za oceno stanja gostote pasti so uporabili enačbo, ki je tesno povezana s koncentracijo dopanta v plasti. Dobljeni rezultati so pokazali, da je gostota pasti kritični parameter za oceno maksimalne vrednosti potenciala pregrade. Ta parameter je močno odvisen od velikosti kristalnih zrn in posledično tudi od debeline (širine) kristalnih mej. Prevodne oziroma transportne lastnosti predstavljene s tokom električno nabitih delcev(termioničnim tokom) in efektivna mobilnost prav tako dokazujejo to odvisnost. Poleg tega se dobljeni rezultati dobro ujemajo z eksperimentalno izmerjenimi vrednostmi, podanimi v predhodnih raziskavah.

Ključne besede: pasti, nosilci naboja, koncentracija dopiranja, velikost kristalnih zrn

1 INTRODUCTION

The effect of the grain boundaries on the conduction properties of the polycrystalline films used in various applications, including discrete devices and integrated circuits, has prompted several studies of the carrier transport.[1–7] In the photovoltaic field, an inexpensive polycrystalline solar cell has also received considerable attention by various research groups.[8–12] The grain boundaries in polycrystalline silicon act as carrier migration routes.[13] These boundaries can modify the undesired trap rate, which is considered as one of the most important challenges in these materials.

A lot of defects found at grains boundaries due to incomplete atomic bonds (dangling bonds)[13,14] are supposed to act as traps for the doping atoms as a result of their segregation in the latter. Consequently, trap states are formed, able to trap and immobilize charge carriers. The number of free carriers available for electrical conduction is reduced. As soon as the free carriers freeze, traps become electrically charged and a potential barrier appears[15–22], preventing the movement of a grain carrier to its neighbor, thus, limiting their mobility.[23] This dopant segregation reduces the number of dopant atoms in the grains and the number of active charge carriers decreases. It should be noted that, in terms of grain size and grain boundaries, the crystalline structure of polysilicon films significantly affects the conduction properties even when individual grains are physically small.[23] Understanding the diffusion of dopants in grains and also the grain-boundary segregation is necessary to control the fabrication of devices containing polysilicon layers.

Thus, in this study a graphical method is suggested to determine the potential barrier for which an empirical relationship is used to estimate the density of the trapping states[23] where some modifications have been introduced to check the effects of the grain size and doping concentration in polycrystalline materials.

2 METHODOLOGY

The used model is based on the principle developed by Seto and other researchers who succeeded him.[19,22,24–26] The formation of trap states (N_t) is due to the existence of a large number of defects at grain boundaries, able to trap charge carriers and immobilize them. The trapped charges are compensated by charged depletion regions surrounding the grain boundaries, which cause a curvature of the energy bands and the re-

*Corresponding author's e-mail:
smerabet@univ-jijel.dz (Souad Merabet)

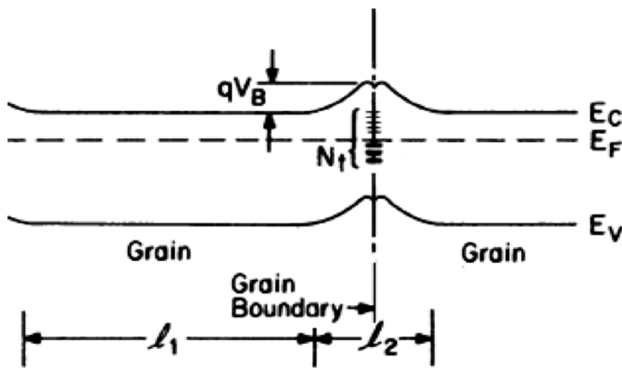

Figure 1: Energy-band diagram of the *n*-type silicon[22]

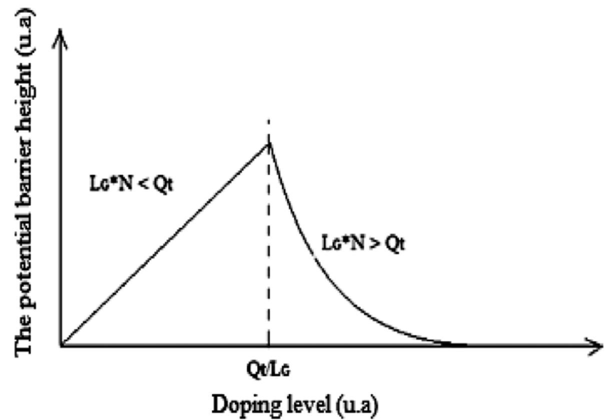

Figure 2: Potential barrier height as a function of grain-boundary doping

sulting potential barriers (see **Figure 1**),[22] impeding the movement of carriers from one crystallite to another.

This model, which was established by the researchers as shown in **Figure 2**, predicts a strong resistivity below the critical doping concentration N^* (cm^{-3}), which drops rapidly for $N > N^*$. The principle can be summarized as follows:

For $N \approx N^*$, the concentration of free carriers is low and the resistivity is high (see Equation (1)):

$$L_G \times N < Q_t \Rightarrow V_b = q \times \frac{L_G^2 \times N}{8 \times \varepsilon_0 \times \varepsilon_{Si}} \quad (1)$$

where V_b is the potential barrier (V), L_G is the average grain size (nm), N is the dopant concentration (cm^{-3}), ε_{Si} is the silicon dielectric permittivity, q is the elementary charge (C), and Q_t is the charge on the traps (cm^{-2}).

For $N < N^*$, the potential barrier at grain boundaries (created by the present defects) increases, making the movement of the carriers from one grain to another more difficult. Then the effective mobility decreases and the resistivity remains high. The potential barrier is at its maximum value, as shown by Equations (2) and (3):

$$L_G \times N = Q_t \Rightarrow N = N^* \rightarrow V_b = q \times \frac{L_G^2 \times N^*}{8 \times \varepsilon_0 \times \varepsilon_{Si}} = q \times \frac{Q_t^2}{8 \times \varepsilon_0 \times \varepsilon_{Si} \times N^*} \quad (2)$$

$$\Rightarrow N = N^* = \frac{Q_t}{L_G} \quad (3)$$

For $N > N^*$, the concentration of free carriers increases and the height of the potential barrier decreases, as expressed by Equation (4). The resistivity decreases rapidly as the doping concentration increases until it reaches that of the monocrystalline silicon.

$$L_G \times N > Q_t \Rightarrow V_b = q \times \frac{Q_t^2}{8 \times \varepsilon_0 \times \varepsilon_{Si} N} \quad (4)$$

Where $\varepsilon_0 = 8.85 \times 10^{-12}$ F/m and $\varepsilon_{Si} = 11.68$.

In accordance with these concepts, the effect of the variation in the grain size and doping concentration on the assessment of the potential barrier height, thermionic current and effective mobility is studied below.

Several models have been proposed to describe the density of trap states N_t (cm^{-2}). In this work, an empirical equation established during previous work[24] is used with some modifications:

$$N_t = (35 + 2.55 \times L_G^{-\alpha}) \times 10^{10} \quad (5)$$

These changes refer to the value of parameter α, according to which the calculations are strictly dependent on the doping rate; the chosen values have been verified and validated during the comparison with the previous experimental results,[19,24] and the details of the calculations are reported in **Table 1**. The obtained values show that the critical doping concentration N^* (cm^{-3}) and parameter α evolve in proportion to the increase in the dopant concentration of the sample.

Two case studies were considered. In the first step, a choice about the doping rates used during the previous

Table 1: Parameters needed for the simulation

L_G (× 10^{-7} cm)	Doping concentration (cm^{-3})	α	Trapping state density N_t	
			Experimental values (× 10^{12} cm^{-2}) (Ref. [19])	Computed values (× 10^{12} cm^{-2})
20	5 × 10^{18}	0.3533	2.98	2.9802
	7 × 10^{18}	0.3630 (Ref. [20])	/	3.3372
	1 × 10^{19}	0.3649	3.41	3.4126
	5 × 10^{19}	0.3704	3.64	3.6418

works was made[18,23] to validate the proposed calculation method with a fixed grain size of about 20 nm. In the second step with a fixed doping concentration, the grain size was varied.

3 RESULTS AND DISCUSSION

3.1 Potential barrier height

The computed variations in the potential barrier height for different doping concentrations are shown in **Figure 3a**, calculated with Equations (1), (3) and (4) above. The potential barrier increases linearly as the doping level reaches a maximum value, due to the addition of more impurity atoms to the traps. The grain-boundary traps increase the potential barrier and decrease the carrier density of the grain.[27] After this, the potential barrier decreases rapidly with a high doping concentration because the traps are filled and the free-carrier concentration increases. This is very consistent with the previous findings.[28–30]

Following the line along the doping axis, which corresponds to the layer doping along the curve, allows us to determine the value corresponding to the potential barrier represented by the intersection point (see **Figure 3b**). **Table 2** shows the obtained results, which correspond well with the experimental values found in the literature,[19] and the values are mostly identical. They show that the trap density and the potential barrier evolve proportionally with the increase in the dopant concentration of the polysilicon layer at a constant average grain size.

Likewise, as before, the doping is set to 1×10^{19} (cm^{-3}). The first value of the grain size is 20 nm so that we can compare and then validate the results obtained for the new, randomly chosen grain sizes. The computed values are represented in **Figure 4a**. The critical concentration N^* is found to decrease with the increasing grain size.

Corresponding to the different grain sizes selected, the values of the potential barrier are determined, as before, as shown in **Figure 4b**, by the point of intersection of the line acrossing the various curves drawn and the corresponding doping axis to 1×10^{19} (cm^{-3}). In summary, the obtained results are reported in **Table 3**. It is found that the density of trapping states and the maximum value of the potential barrier decrease with the increasing grain size at grain boundary levels, thus facilitating the passage of carriers from one grain to another;

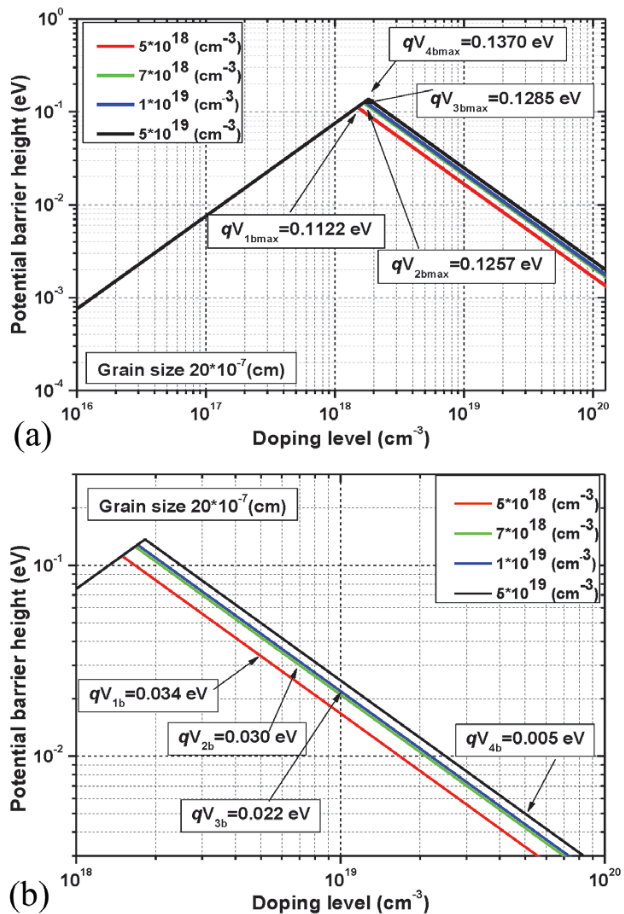

Figure 3: a) Potential barrier height as a function of the doping level, and b) potential barrier values

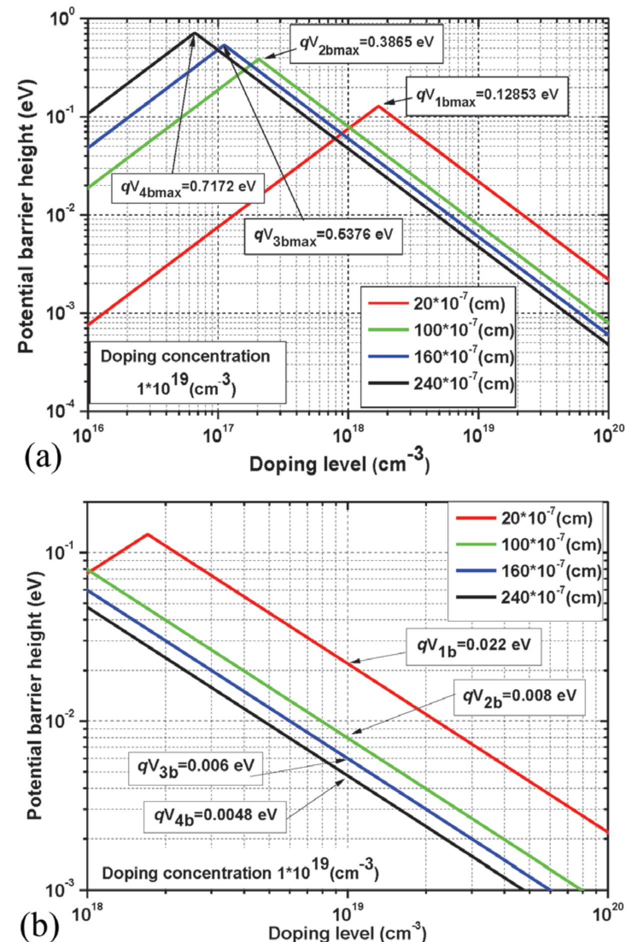

Figure 4: a) Potential barrier height as a function of the grains size, and b) potential barrier values

Table 2: Obtained results as a function of the doping concentration

Doping concentration (cm^{-3})	N^* ($\times 10^{18}$ cm^{-3})	Maximum height of potential barrier qV_{bmax} (eV)	Potential barrier qV_b (eV) (Ref. [19])	Potential barrier qV_b (eV)	Variation $q(V_b - V_{b(i-1)})$ (eV)
5×10^{18}	1.49	0.1122	0.0335	0.0334	0.0034
7×10^{18}	1.67	0.1257	/	0.030	
1×10^{19}	1.7063	0.1285	0.022	0.022	0.008
5×10^{19}	1.82	0.1370	0.005	0.005	0.017

this is explained with the decrease in the disorder in larger grains.[22,26–31]

3.2 Thermionic current density

The current flow in polycrystalline materials is limited by the carrier movement across the grain boundary barrier rather than the current flow in the grains themselves.[32] The maximum flux of carriers, considered as free particles by several models,[33–36] is provided by the thermionic emission above the potential barrier depending on its height rather than its shape. The thermionic current density across the height of the barrier is given by the number of carriers that have sufficient energy under an applied voltage to move towards the grain boundaries that can overcome this barrier.[19,32]

Figure 5a shows the variation in the thermionic current density according to the applied potential and the change in the doping level. The choice of the applied potential values (U_a) must satisfy the ones imposed by the models.[19,32] Therefore, U_a is the polarization across the sample divided by the number of grains, assuming all the grain boundaries are identical.[32] In general, the applied bias voltage is non-uniformly divided between the two sides of a grain boundary. However, for low voltages, approximately half of this voltage appears on each side.[32] The thermionic current density is initially high at low doping rates due to a complete depletion of the grains and the potential barriers are not yet formed as a result of the partial filling of the traps due the low doping levels. At increasing doping levels, the thermionic current den-

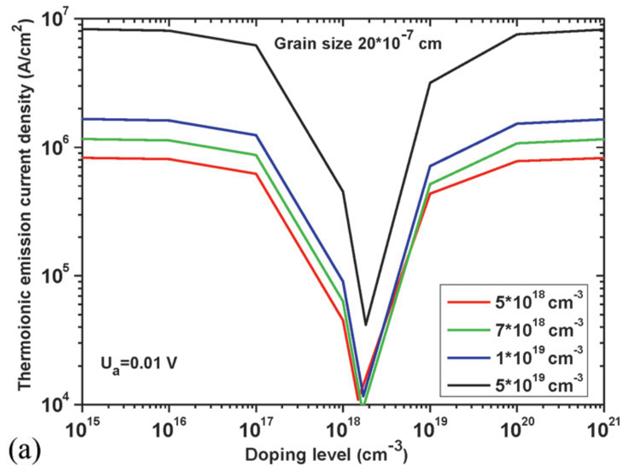

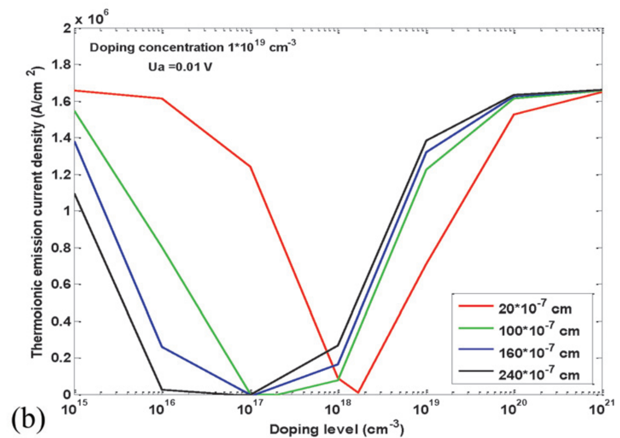

Figure 5: Thermionic-emission current density as a function of: a) doping concentration, b) grain size

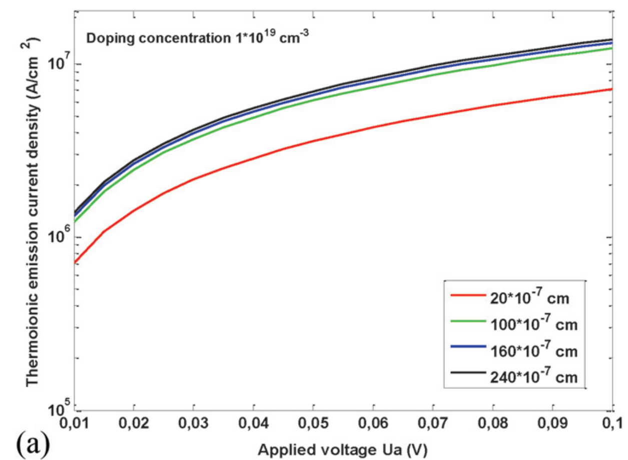

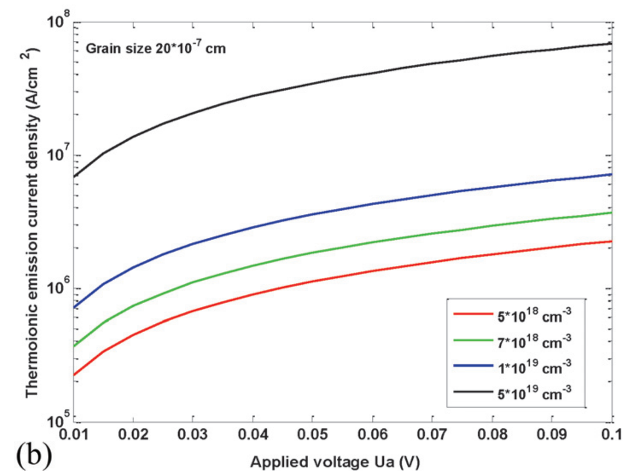

Figure 6: Thermionic-emission current density as a function of applied voltage and: a) doping concentration, b) grain size

Table 3: Obtained results as a function of the grain size

Grain size ($\times 10^{-7}$ cm)	Trapping state density N_t ($\times 10^{12}$ cm^{-2})	N^* (cm^{-3})	Maximum height of potential barrier qV_{bmax} (eV)	Potential barrier qV_b (eV)	Variation $q(V_{bi}–V_{b(i-1)})$ (eV)
20	3.4126	1.7063×10^{18}	0.12853	0.022	0.014
100	2.0523	2.0523×10^{17}	0.3865	0.008	
160	1.7840	1.115×10^{17}	0.5376	0.006	0.002
240	1.5868	6.6117×10^{16}	0.7172	0.0048	0.0012

sity decreases, and a minimum value dip occurs at a critical doping concentration when the barrier height is maximum, and, at higher doping levels, the barrier height is reduced, allowing an increase in the thermionic current density resulting from the rapid conduction.

A strong shift was observed between the four curves due to the increase in the doping concentration, which led to a decrease in the potential barrier height, verified by the results obtained from **Table 2**. The observed deviation between the curves was found to be in reasonable agreement with the theoretical predictions as a function of the doping concentration.

As the grain size increases at a fixed doping concentration (see **Figure 5b**) and at low doping levels, a thermionic current density value decrease dip occurs at a critical doping concentration. This decrease highly depends on the height of the corresponding potential barrier. It is worth noting that the corresponding curves at low grain sizes, 20 nm and 100 nm, are higher than those at higher grains sizes. These results are consistent with those shown in **Figure 4**. For any grain size, the position of the minimum value depends on the maximum value of the potential barrier and the density of the trapping states; after this value, the barrier decreases for high doping levels and the current density increases proportionally with the grain size.

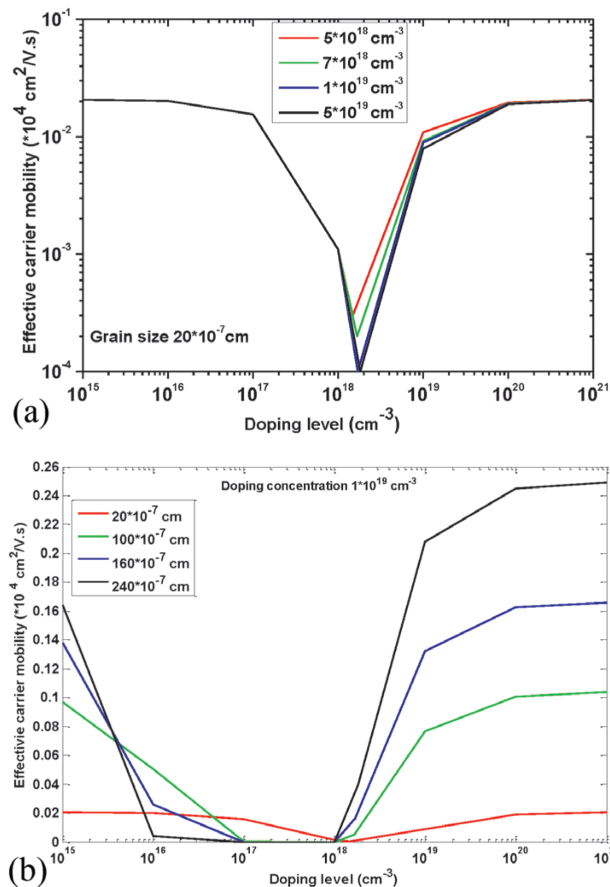

Figure 7: Effective carrier mobility as a function of: a) doping level, b) grain size

The thermionic current density versus the applied potential change is shown in **Figure 6**. The current density grows weakly at low voltages. This is attributed to the fact that the carriers moving through the grain boundaries have more opportunities to be trapped at the trapping sites. As the applied voltage rises, the effect of the barrier becomes insignificant.[37,38] The carriers have enough energy to bypass the barrier, so the current density increases rapidly.

3.3 Effective mobility carrier

Effective mobility describes the ease of the carrier movement from one grain to another and also the restriction of the current flow by the potential barrier at grain boundaries.[15] Therefore, it depends considerably on the doping concentration. In this last part of our work, the mobility is plotted in **Figure 7** as a function of the doping-concentration variation in the first stage and as a function of the grain-size variation in the second stage.

The mobility plot is remarkably similar to the one for the thermionic current density. It can be clearly seen that the mobility presents the minimum value for the critical doping concentration N^*, which decreases at low doping (high V_b) and then increases at doping concentrations above N^* (low V_b). This result is in good agreement with the other research findings published in the literature.[24] The evolution of the obtained curves agrees well with the curve results from **Figures 3** and **4**.

The observed discrepancy between the curves obtained for the effective mobility and thermionic current density at high doping levels (see **Figures 6** and **7**) is attributed to the difference in the obtained potential-barrier values at the grain boundaries. When the doping concentration increases at a fixed grain size, the discrepancy becomes important, increasing from 0.0034 eV to 0.008 eV, and from 0.008 eV to 0.017 eV (see **Table 2**). It decreases from 0.014 eV to 0.002 eV, and from

0.002 eV to 0.0012 eV when the grain size increases with a constant doping concentration (see **Table 3**).

4 CONCLUSIONS

In this study, the method used to determine the potential barrier as a function of trapping density states in polycrystalline layers was verified by feeding calculated parameters into the plotting of equations and comparing them with the experimental data reported in the previous research works. Almost all the results were in agreement.

The obtained results showed that when the layers have the same grain size, the states of trapping density and critical concentration are proportional to the increasing doping concentration (see **Table 2**) and the corresponding potential barrier is inversely proportional. An increasing discrepancy is observed between the thermionic current density curves due to the growing difference between the calculated potential barrier values (from 0.0034 eV to 0.017 eV). This is explained by the fact that the trapping levels become pretty full and the rate of free carriers increases, inducing a barrier reduction.

Also, when the layers have the same doping concentration, the density states of traps, the critical concentration and the corresponding potential barrier are inversely proportional to the increasing grain size (see **Table 3**). The spacing between the thermionic current density curves becomes small with the grain growth, which is also related to the decreasing difference between the calculated potential barrier values. This may be due to the reduced number and width of the grain boundaries in the layers.

Hence, increased grain size and doping concentration help to reduce the number of grain boundaries, resulting in a reduced potential barrier and improved transport properties. These results are in good agreement with the other research findings published in the literature.

Acknowledgement

This work was supported by the Algerian Ministry of Higher Education and Scientific Research. We are indebted to all the members of the LER Laboratory of the Jijel University for their services and assistance, as well as to our research teams in Jijel and Constantine.

5 REFERENCES

[1] B. Olyaeefar, S. Ahmadi-Kandjani, A. Asgari, Classical modelling of grain size and boundary effects in polycrystalline perovskite solar cells, J. Solar Energy Materials and Solar Cells, 180 (**2018**), 76–82, doi:10.1016/j.solmat.2018.02.026

[2] S. Park, M. A. Shehzad, M. F. Khan, G. Nazir, J. Eom, H. Noh, Y. Seo, Effect of grain boundaries on electrical properties of polycrystalline graphene, J. Carbon, 112 (**2017**), 142–148, doi:10.1016/j.carbon.2016.11.010

[3] M. Hogyoku, T. Izumida, H. Tanimoto, N. Aoki, S. Onoue, Grain-boundary-limited carrier mobility in polycrystalline silicon with negative temperature dependence: modeling carrier conduction through grain-boundary traps based on trap-assisted tunneling, Jpn. J. Appl. Phys., 58 (**2019**), SBBA01, doi:10.7567/1347-4065/aaf7fa

[4] M. V. Frischbier, H. F. Wardenga, M. Weidner, O. Bierwagen, J. Jia, Y. Shigesato, A. Klein, Influence of dopant species and concentration on grain boundary scattering in degenerately doped In_2O_3 thin films, J. Thin Solid Films, Part B, 614 (**2016**), 62–68, doi:10.1016/j.tsf.2016.03.022

[5] L. Carnel, I. Gordon, K. Van Nieuwenhuysen, D. Van Gestel, G. Beaucarne, J. Poortmans, Defect passivation in chemical vapour deposited fine-grained polycrystalline silicon by plasma hydrogenation, J. Thin Solid Films, 487 (**2005**), 147–151, doi:10.1016/j.tsf.2005.01.081

[6] S. Merabet, M. Boukezzata, Analysis of boron profiles as function of nitrogen content in silicon, J. Thin Solid Films, 690 (**2019**), 137537, doi:10.1016/j.tsf.2019.137537

[7] Y. Zhao, Q. Song, H. Ji, W. Cai, Z. Liu, Y. Cai, Multi-scale modeling method for polycrystalline materials considering grain boundary misorientation angle, Materials & Design, 221 (**2022**), 110998, doi:10.1016/j.matdes.2022.110998

[8] K. Sharma, Study of photovoltaic properties of silicon solar cell and their dependence on grain boundaries, J. Advanced Research in Engineering and Technology, 11 (**2020**) 9, 1112–1119, doi:10.34218/ijaret.11.9.2020.111

[9] A. Abass, B. Maes, D. Van Gestel, K. Van Wichelen, M. Burgelman, Effects of inhomogeneous grain size distribution in polycrystalline silicon solar cells, Energy Proc., 10 (**2011**), 55–60, doi:10.1016/j.egypro.2011.10.152

[10] A. Abass, D. Van Gestel, K. Van Wichelen, B. Maes, M. Burgelman, On the diffusion length and grain size homogeneity requirements for efficient thin-film polycrystalline silicon solar cells, J. Phys. D: Appl. Phys., 46 (**2012**), 045105, doi:10.1088/0022-3727/46/4/045105

[11] M. Burgelman, P. Nollet, S. Degrave, Modelling polycrystalline semiconductor solar cells, Thin Solid Films, 361 (**2000**), 527–532, doi:10.1016/S0040-6090(99)00825-1

[12] Y. Yanfa, Y. Wan-Jian, W. Yelong, S. Tingting, P. R. Naba, L. Chen, J. Poplawsky, Z. Wang, J. Moseley, H. Guthrey, H. Moutinho, S. J. Pennycook, M. M. Al-Jassim, Physics of grain boundaries in polycrystalline photovoltaic semiconductors, J. Appl. Phys., 117 (**2015**) 112807, doi:10.1063/1.4913833

[13] B. Gaury, P. M. Haney, Charged grain boundaries and carrier recombination in polycrystalline thin film solar cells, Physical Review Applied, 8 (**2017**), 054026, doi:10.1103/PhysRevApplied.8.054026

[14] R. Gegevicius, M. Franckevicius, V. Gulbinas, The role of grain boundaries in charge carrier dynamics in polycrystalline metal halide perovskites, Eur. J. Inor. Chem., (**2021**) 35, 3519–3527, doi:10.1002/ejic.202100360

[15] C. Persson, A. Zunger, Anomalous grain boundary physics in polycrystalline $CuInSe_2$: the existence of a hole barrier, Physical Review Letters, 91 (**2003**) 26, 266401, doi:10.1103/PhysRevLett.91.266401

[16] R. Herberholz, U. Rau, H. W. Schock, T. Haalboom, T. Gödecke, F. Ernst, C. Beilharz, K. W. Benz, D. Cahen, Phase segregation, Cu migration and junction formation in $Cu(In,Ga)Se_2$, Eur. Phys. J. Appl. Phys., 6 (**1999**) 2, 131–139, doi:10.1051/epjap:1999162

[17] A. Niemegeers, M. Burgelman, R. Herberholz, U. Rau, D. Hariskos, Model for electronic transport in $Cu(In,Ga)Se_2$ solar cells, Prog. Photovolt. Res. Appl., 6 (**1998**) 6, 407–421, doi:10.1002/(SICI)1099-159X(199811/12)6:6<407::AID PIP230>3.0.CO;2-U

[18] M. J. Romero, K. Ramanathan, M. A. Contreras, M. M. Al-Jassim, R. Noufi, P. Sheldon, Cathodoluminescence of $Cu(In,Ga)Se_2$ thin films used in high-efficiency solar cells, Appl. Phys. Lett., 83 (**2003**), 4770, doi:10.1063/1.1631083

[19] J. Y. W. Seto, The electrical properties of polycrystalline silicon films, Journal of Applied Physics, 46 (**1975**) 12, 5247–5254, doi:10.1063/1.321593

[20] T. Kamins, Polycrystalline silicon for integrated circuits applications, Stanford University, 1988, Kluwer Academic Publishers

[21] E. Canessa, V. L. Nguyen, Non-linear I–V characteristics of double Schottky barriers and polycrystalline semiconductors, Physica B: Condensed Matter, 179 (**1992**) 4, 335–341, doi:10.1016/0921-4526(92)90634-5

[22] F. Greuter, G. Blatter, Electrical properties of grain boundaries in polycrystalline compound semiconductors, Semicond. Sci. Technol,. 5 (**1990**) 2, 111, doi:10.1088/0268-1242/5/2/001

[23] S. Tsurekawa, K. Kido, T. Watanabe, Measurements of potential barrier height of grain boundaries in polycrystalline silicon by Kelvin probe force microscopy, J. Philosophical Magazine Letters, 85 (**2005**) 1, 41–49, doi:10.1080/09500830500153859

[24] N. Gupta, B. P. Tyagi, An analytical model of the influence of grain size on the mobility and transfer characteristics of polysilicon thin-film transistors (TFTs), J. Physica Scripta, 71 (**2006**) 2, 225–228, doi:10.1238/Physica.Regular.071a00225

[25] J. P. Colinge, E. Demoulin, F. Delannay, M. Lobet, J. M. Temerson, Grain size and resistivity of LPCVD polycrystalline silicon films, J. Electrochem. Soc., 128 (1**981**), 2009–2014, doi:10.1149/1.2127785

[26] B-H. Yan, B. Li, R-H. Yao, W-J. Wu, A physics-based effective mobility model for polycrystalline silicon thin film transistor considering discontinuous energy band at grain boundaries, Jpn. J. Appl. Phys., 50 (**2011**), 094302, doi:10.1143/jjap.50.094302

[27] J. G. Lee, T. W. Kim, Effects of the grain boundary and interface traps on the electrical characteristics of 3D NAND flash memory devices, J. Nanosci. Nanotechnol., 18 (**2018**) 3, 1944–1947, doi:10.1166/jnn.2018.15000

[28] G. Baccarani, B. Riccò, G. Spadini, Transport properties of polycrystalline silicon films, J. Appl. Phys., 49 (**1978**), 5565–5570, doi:10.1063/1.324477

[29] T. Takagi, F. Koyama, K. Iga, Potential barrier height analysis of AlGaInP multi-quantum barrier (MQB), Jpn. J. Appl. Phys., 29 (**1990**), L1977, doi:10.1143/JJAP.29.L1977

[30] H. Dong, J. Sun, S. Ma, J. Liang, T. Lu, Z. Jia, X. Liu, B. Xu, Effect of potential barrier height on the carrier transport in InGaAs/GaAsP multi-quantum wells and photoelectric properties of laser diode, J. Phys. Chem. Chem. Phys., 18 (**2016**) 9, 6901–6912, doi:10.1039/C5CP07805A

[31] A. Shamir, I. Amit, D. Englander, D. Horvitz, Y. Rosenwaks, Potential barrier height at the grain boundaries of a poly-silicon nanowire, Nanotechnology, 26 (**2015**) 35, 355201, doi:10.1088/0957-4484/26/35/355201

[32] S. D. Brotherton, Introduction to thin film transistors, Chapter 8, Poly-Si TFT Performance, Springer International Publishing, 2013, Switzerland

[33] A. T. Hatzopoulos, D. H. Tassis, N. A. Hastas, C. A. Dimitriadis, G. Kamarinos, On-state drain current modeling of large-grain poly-Si TFTs based on carrier transport through latitudinal and longitudinal grain boundaries, IEEE Transactions on Electron Devices, 52 (**2005**) 8, 1727–1733, doi:10.1109/ted.2005.852732

[34] H. Ikeda, Analysis of grain boundary induced nonlinear output characteristics in polycrystalline-silicon thin-film transistors, Jpn. J. Appl. Phys., 45 (**2006**) 3R, 1540, doi:10.1143/JJAP.45.1540

[35] M. Wang, M. Wong, An effective channel mobility-based analytical on-current model for polycrystalline silicon thin-film transistors, IEEE Transactions on Electron Devices, 54 (**2007**) 4, 869–874, doi:10.1109/ted.2007.891248

[36] M. Wong, T. Chow, C. C. Wong, D. Zhang, A quasi two-dimensional conduction model for polycrystalline silicon thin-film transistor based on discrete grains, IEEE Transactions on Electron Devices, 55 (**2008**) 8, 2148–2156, doi:10.1109/ted.2008.926277

[37] A. Valletta, P. Gaucci, L. Mariucci, A. Pecora, M. Cuscunà, L. Maiolo, G. Fortunato, Threshold voltage in short channel polycrystalline silicon thin film transistors: Influence of drain induced barrier lowering and floating body effects, J. Appl. Phys, 107 (**2010**) 7, 074505, doi:10.1063/1.3359649

[38] B. Du, C. Han, Z. Li, C. Han, J. Li, M. Xiao, Z. Yang, Effect of polarity-reversal voltage on charge accumulation and carrier mobility in silicone rubber/silicon carbide composites, IET Sci. Meas. Technol., 15 (**2021**), 184–192, doi:10.1049/smt2.12020